Research Article Open Access

Nermin Kutlu*, Halil Oturak

The Optical and Crystallite Characterization of Bilayer TiO_2 Films Coated on Different ITO layers

https://doi.org/10.1515/chem-2018-0135
received February 1, 2018; accepted September 1, 2018.

Abstract: Titanium dioxide(TiO_2) is a well-known material which is non-toxic with efficient photoactivity, high stability, low-cost and corrosion-resistant. Up to today's technology, TiO_2 films are coated for various applications in the scientific area. In this study, bilayer TiO_2 films were coated on indium tin oxide(ITO) layers that have different characteristic properties. The devices designed as home-made of Direct Current Magnetron Sputtering (DCMS) and Spray Pyrolysis Deposition (SPD) coating methods were used to coat the first and second layers of bilayer TiO_2 films, respectively. The optical and crystalline characterizations of bilayer TiO_2 films were analyzed by UV-VIS spectroscopy and XRD techniques. The XPS spectrum showed that O_2 molecules simply oxidize from Ti^{3+} to Ti^{4+} after SPD coating method. The characterization results of TiO_2 films showed change in optical band gap value and crystalline structure of TiO_2 bilayer.

Keywords: bilayer TiO_2 (87.16.D); crystalline (61.66.Dk); optical (78.20.Ci); photoanodes; spectroscopy (07.57.c).

1 Introduction

Indium tin oxide (ITO) is known as transparent conducting material due to its wide optic band gap and numerous charge carriers in its conduction band. It is commonly used in application fields such as thermal collectors, mirrors, gas sensors, photodetectors, solar cells, OLEDs and liquid crystal displays**.** However, Titanium dioxide (TiO_2) is a semiconductor material which has wide optic band gap, non-toxic, low-cost, efficient photoactivity, high stability, corrosion-resistance and transmittance in the visible region of the electromagnetic spectrum [1-3]. TiO_2 films should have properties required in application fields such as the media layer for transferring of electrons in the DSSCs, the photo-catalysts for H_2 production, the photoresponse layer of UV detector, the hole blocking, hole transporter or emissive layer of OLEDs, the gas sensing layer of gas sensors, the UV absorbing nanoparticles of UV protection fabrics, for the reduction of water pollutions, in the field of biofuel production, electrodes in Li-ion batteries etc. [4-15]. According to results reported for these applications, the optical and crystal properties of TiO_2 to be used in application fields are too important to gain efficiency in these fields.

TiO_2 has three crystallite types which are brookite, anatase and rutile. Titanium has oxidation states of +2, +3 and +4 such as Ti^{2+}, Ti^{3+} and Ti^{4+}. Out of these, Ti^{3+} has surface defects (TSD) in anatase form enhance photocatalytic effect by extending of its absorption wavelength from UV to visible region of the electromagnetic spectrum**[16].** Electron and holes are generated by light adsorbed with TiO_2 in the reaction (1)**[17].**

$$TiO_2 + h\nu \rightarrow TiO_2(e^-_{CB} + h^+_{VB}) \quad (1)$$

$$Ti^{4+} + e^-_{CB} \rightarrow Ti^{3+} \quad (2)$$

$$O_2 + e^-_{CB} \rightarrow O_2^- \quad (3)$$

$$O_2 + Ti^{3+} \rightarrow O_2^- + Ti^{4+} \quad (4)$$

When the photogenerated electrons reach to TiO_2 surface, they are captured by Ti^{4+} and cause Ti^{3+} as shown in reaction (2) [18]. They can be captured by oxygen molecules adsorbed on the TiO_2 surface and superoxide anions form as reaction (3) [19] and so Ti^{3+} formation can be prevented. Simultaneously, O_2 molecules simplify oxidation from Ti^{3+} to Ti^{4+} reaction (4) [20] therefore, Ti^{4+} ions are formed instead of Ti^{3+} ions at the TiO_2 surface [21].

DCM sputtering is physical depositing method that is used by changing depositing conditions such as sputtering power, sputtering pressure, gases, gas flow, gas ratio, deposition rate and temperature etc. Stamate

***Corresponding author: Nermin Kutlu,** Süleyman Demirel University, Physics Department, Isparta, Turkey,
E-mail: kutlugulnermin@gmail.com
Halil Oturak: Süleyman Demirel University, Physics Department, Isparta, Turkey

et al. introduced TiO_2 films with different optic band gap energy (E_{OBG}) in different DCM sputtering conditions [22]. Singh and Kaur showed that E_{OBG} value of TiO_2 films coated by DCMS decreased with increasing sputtering power (W) from 50 W to 200 W. Moreover, they clarifies that while crystallite size (nm) and film thickness (nm) increase with increasing sputtering power, transmittance of TiO_2 films decreases [23].

Spray Pyrolysis Deposition (SPD) method is commonly used for obtaining the porous TiO_2(p-TiO_2). There are some external factors such as post-annealing, temperature of hot plate during coating and solution [24] that affect properties of TiO_2 films such as E_{OBG}, surface structure, crystallite size, crystallite structure etc. [25-27].

In this study, bilayer TiO_2 films were coated in the same DCMS and SPD conditions on ITO layers with different E_{OBG} and crystal structure. The optical and crystallite characterizations of bilayer TiO_2 films were analyzed by UV-VIS spectroscopy and XRD devices. The aim of this study is to show that ITO layers with different properties affect properties of bilayer TiO_2 films.

2 Experimental

2.1 Coating of Bilayer TiO_2 Films

A metallic titanium target the purity of 99.5% with diameter of 60 mm used to obtain the dense layer TiO_2 film. The three chemical materials, which are titanium(IV) isopropoxide $Ti(O\text{-}iPr)_4$, ethanol, acetylacetone was used to coat the p-TiO_2 film. All chemicals were purchased from Sigma–Aldrich and were used as received.

ITO films with different property were used as glass substrates of bilayer TiO_2 films. Disk of TiO_2 were used as sputtering targets to deposit first layer of TiO_2 on ITO surface which was also the first layer of TiO_2-based bilayer photoanode. The sputtering chamber was pumped down to 3×10^{-5} mbar and then high purity Ar (4 sccm=4 atm cm^3/min) were introduced into vacuum chamber as working ambience by mass flow control system. The deposited process was applied at 3×10^{-2} mbar. A constant DC power at 150 W was applied to the target. Substrate temperature was kept 23°C during deposition. Before deposition of all the samples, the surface of target was cleaned by 10 min at a pressure of sputtering. Sputtering time was 1 hour. This was in order to remove the possible contaminations.

SPD method was used to coat the second layer of titania on sputtered titania film which is second layer of TiO_2-based bilayer photoanode. This method allows in obtaining rougher films, with higher surface areas, compared with those obtained by magnetron sputtering, this being a prerequisite in the construction of a Grätzel solar cell. The solution as in the receipt to coat the second layer of titania *via* SPD method is prepared to be consistant in [1]: titanium(IV) isopropoxide (0.1 mol/L) and acetylacetone in a molar ratio of 1:2 in ethanol [25]. The spraying process was performed in the following after preparing the solution. This second layer of TiO_2 was deposited by spraying an appropriate solution on the samples maintained at 387 K during the spraying procedure. The sprayer was placed at 18 cm in front of a heated substrate holder (inclined at 55° with respect to the horizontal plane). The spraying was performed in the following sequence: 10s spray, 20s break, which was repeated 3 times. A 10 min break was followed by each spray. The obtained films were cooled till the room temperature, together with the heater. The pyrolytic reaction takes place on the substrate, leading to a nano-crystalline metal oxide. The as-deposited thin films were then compacted by placing the samples in the middle of a temperature-controlled furnace. All of the deposited samples were heated at 450°C for 3 hours to remove their chemical contaminants after their coating process.

2.2 Characterisation of Bilayer TiO_2 Films

The first characterization of TiO_2-based bilayer films was done to determine their thickness by using a surface Tencor Alpha Step 500 profilometer.

UV-VIS characterization was done by using Analytic Jena Speedcord S600 Spectroscopy. Optic band gap energy of thin films was determined by Equation 1 [28].

$$E_{OBG} = \frac{h \times c}{\lambda} = \frac{1240 eV.nm}{\lambda} \quad (1)$$

Absorbance of light is given by Equation 2.

$$A(\lambda)=\varepsilon(\lambda)dc \quad (2)$$

This Equation 2 is called as Lambert-Beer Law [29] .In this Equation 2, A is absorbance; ε is molecular extinction coefficient; d is path length or thickness; c is concentration of the molecule. Increasing d value in Equation 2 due to cause the increasing absorbance is an important parameter.

The crystallite size has been calculated by using Debye-Scherer formula in the Equation 3 [30].

$$D = \frac{0.9\lambda}{\beta_{1/2}\cos\theta} \quad (3)$$

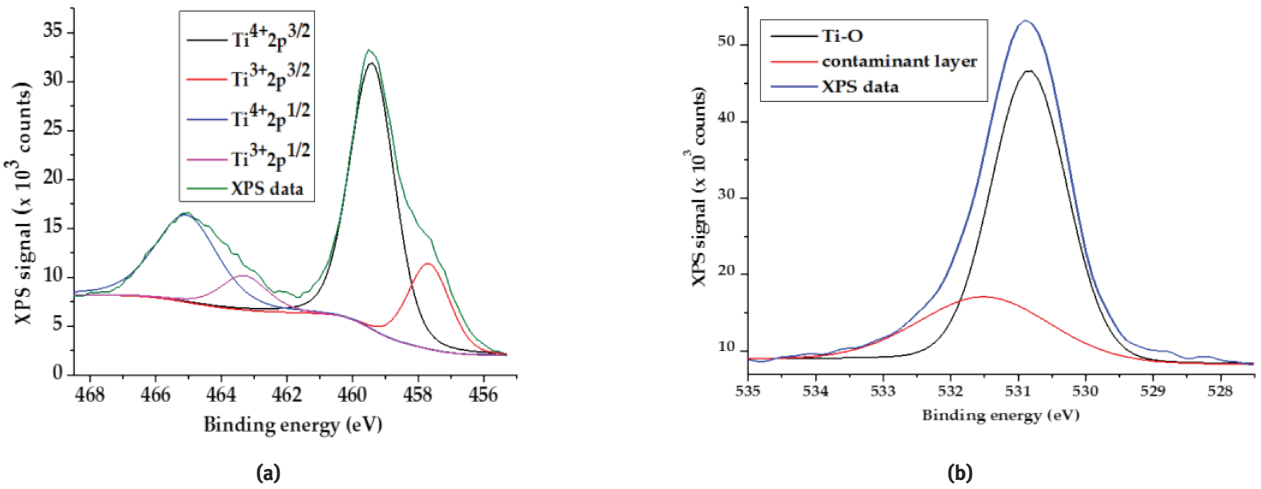

Figure 1: XPS spectras **(a)** Ti 2p **(b)** O 1s of as-deposited d-TiO_2.

In this Equation, λ is 1.542 Å that the wavelength of Cu Kα used for diffraction in XRD, $\beta_{1/2}$ is the full width at half maximum and θ is the angle as degree of pattern with the highest intensity.

$$n\lambda = 2d \sin\theta \tag{4}$$

Equation 4 introduces Bragg Law used to determine the structure of TiO_2 crystals [31]. According this Equation 4, the wavelength of the incident X-ray beam is λ; n is an integer and parallel planes of crystal atoms; the distance between atomic layers in a crystal is d; Bragg's angle is θ. XPS device with mono-chromated Al Kα X-ray (1486.7 eV) was used to determine the composition and electronic state of thin films. The Binding Energy(BE) of thin films is determined by Equation 5.

$$B.E. = h\upsilon - KE - \phi \tag{5}$$

The hν, KE and φ terms in this Equation are the photon energy, kinetic energy and work function [32].

Ethical Approval: The conducted research is not related to either human or animal use.

3 Results

Firstly, difference in method of this study against to traditional coating methods is home-made DCMS and SPD devices used to coat the bilayer TiO_2 samples. The inadequacy in coating process of DCMS device is the vacuum step and the inadequacy in that of SPD device can not homogenously deposit the solution on the materials. XPS spectras given in Figure 1a and Figure 1b are the first characterization result of this study. These spectras clarify the surface compositions and oxidation states of TiO_2-based bilayer photoanodes. As seen in Figure 1a, Ti 2p oxidation state of density(d)-TiO_2 is shown. Owing to the fact that there are both Ti^{4+}(TiO_2) and Ti^{3+}(Ti_2O_3) chemical states in surface of d-TiO_2 coated by magnetron sputtering, d-TiO_2 surface is nonstoichiometric. Figure 1b gives the information about chemical state of O 1s in the d-TiO_2. When Ti^{4+} ions receive electrons, they get convert into trivalent Ti^{3+} ions [18]. On the contrary, as O_2 is adsorbed by TiO_2 surface, Ti^{3+} ions turn to Ti^{4+} ions. The BE, given by Equation 5, of Ti-O(530.84 eV) and contaminant layer(531.51 eV) are obtained from Figure 1b. XPS signal values of Ti-O and contaminant layers against BE values are 46.67×10^3 counts and 17.16×10^3 counts, respectively.

In the Figure 2a, it was shown the Ti 2p oxidation state on the surface of p-TiO_2 coated on d-TiO_2 by SPD method. The p-TiO_2 film coated on d-TiO_2 has stoichiometric properties because of the appearing XPS signal of only Ti^{4+} oxidation state in Figure 2a. The Figure 2b gives the information about chemical state of O 1s in the p-TiO_2. BE of Ti-O(530.90 eV) and contaminant layer(532.19 eV) are calculated from Figure 2b. XPS signal values of Ti-O and contaminant layer are 50.65×10^3 counts and 13.62×10^3 counts, respectively. According to BE values and XPS signals of Ti-O in Figure 1b and in Figure 2b, XPS O 1s spectras of d-TiO_2 and p-TiO_2 are different. While chemical states of O 1s in the d-TiO_2 and p-TiO_2 are the same, O_2 molecules adsorbed by p-TiO_2 surface are plenty more than that by d-TiO_2 surface. Ti^{3+} ions turn to Ti^{4+} ions due

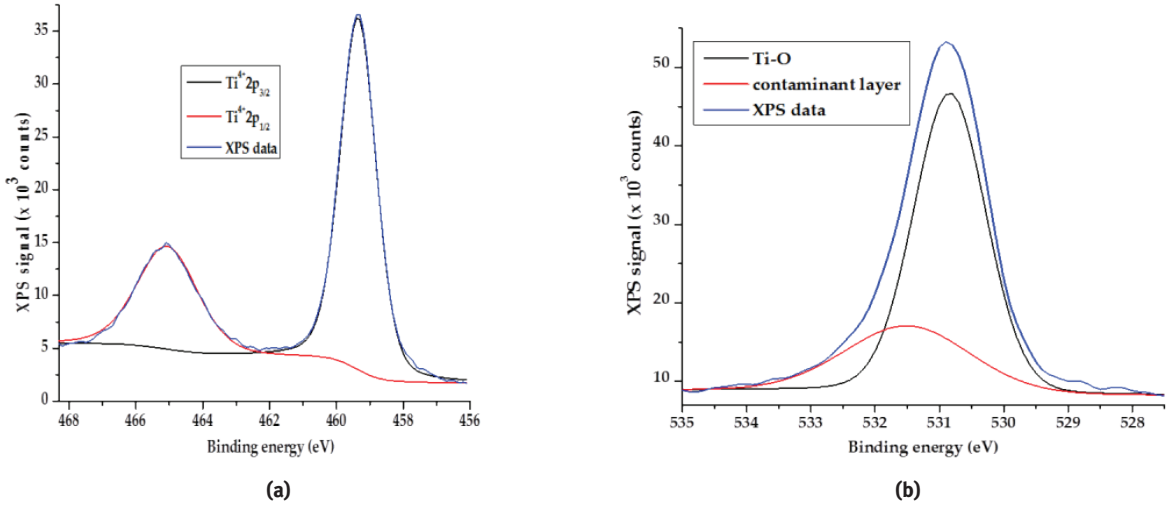

Figure 2: XPS graphs **(a)** Ti 2p **(b)** O 1s of as-deposited p-TiO_2.

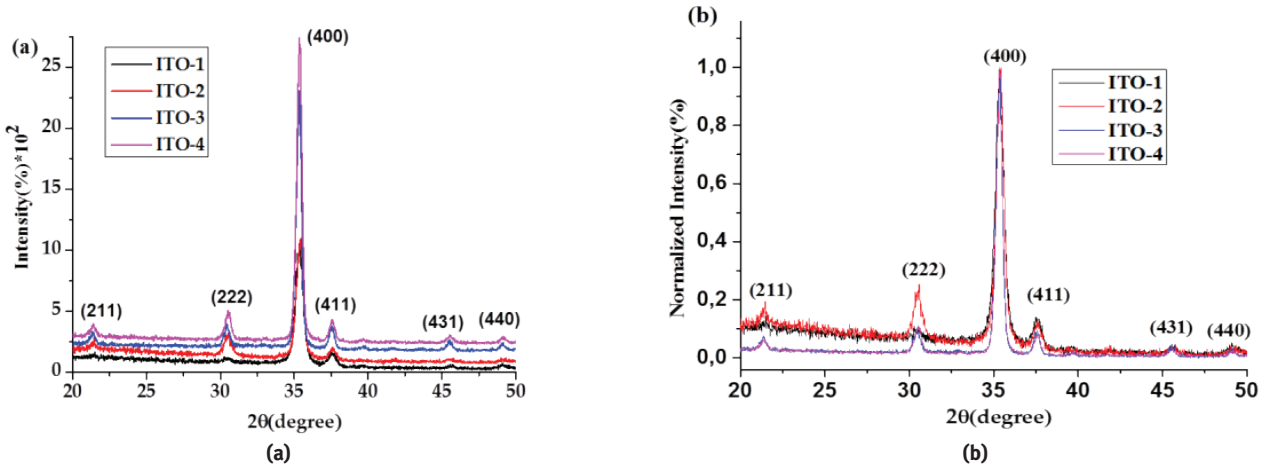

Figure 3: (a) XRD graphs **(b)** Normalized XRD graphs for patterns of ITO films.

Table 1: The atomic(at.%) concentrations of d-TiO_2 and p-TiO_2 layers of TiO_2-based bilayer.

d-TiO_2 layer coated by DCMS method				p-TiO_2 layer coated by SPD method			
TiO_2	C 1s	O 1s	Ar 2p	TiO_2	C 1s	O 1s	Ar 2p
at.%	1.81	65.90	0.82	at.%	2.61	65.21	1.21

to the O_2 molecules adsorbed by TiO_2 surface and thus Ti^{3+} ions are not seen on the p-TiO_2 surface [20,21]. Table 1 gives as atomic(at.%) concentration the chemical composition amount of p-TiO_2 film surface. In the Table 1, chemical composition of d-TiO_2 and p-TiO_2 thin film surfaces is given as atomic (at.%) concentration. According to at.% concentrations in the Table 2, SPD method used to deposit the p-TiO_2 layer on layer of d-TiO_2 did not change the chemical composition of d-TiO_2 layer. These bilayer TiO_2 samples are normally three layers together with ITO substrate as first layer. Figure 3a and Figure 3b give crystallite structure of ITO films.

XRD graphs given patterns of ITO films are shown in Figure 3. XRD patterns of ITO crystal structure are 21°, 30°, 35°, 37°, 45° and 49° with regard to (211), (222), (400), (411), (431) and (440) from (hkl) planes of ITO, respectively**[33]**. While crystallite sizes of ITO-1, ITO-2, ITO-3 and ITO-4 are 17.05 nm, 5.61 nm, 24.37 nm and 22.95 nm respectively, the crystallite size of commercial ITO is smaller than them, between 5 and 10 nm. Moreover, it is expected that the thickness of commercial ITO is thinner than the others, around 100 nm. Because the thickness of films increases with increasing crystallite or grain size [34,35]. While

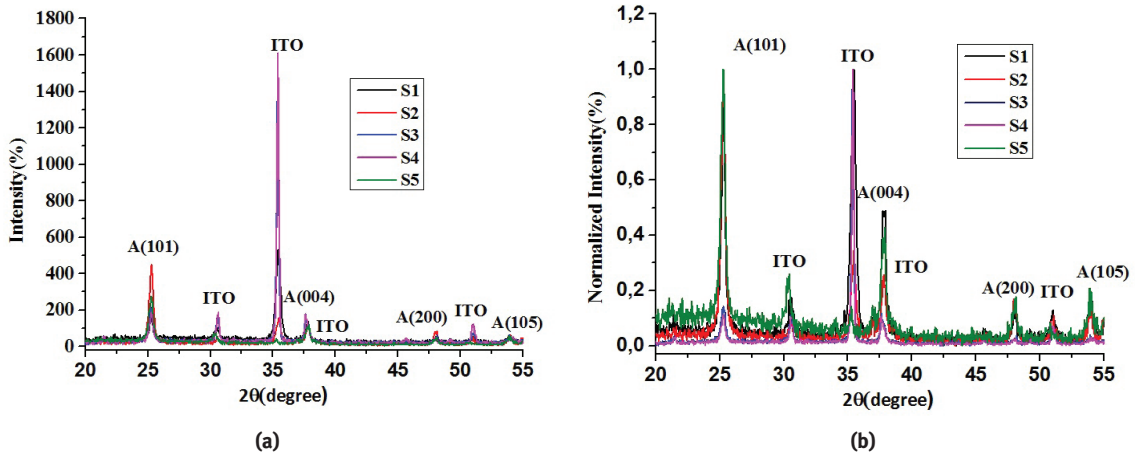

Figure 4: (a) XRD graphs **(b)** Normalized XRD graphs for patterns of bilayer TiO_2 films.

ITO-1 and ITO-3 was annealed at 300°C, ITO-2 and ITO-4 was annealed at 400°C. According to crystallite size values determined by Equation 3, it can be said that crystallite size decreases with increased annealing temperature at 400°C. ITO-1 and ITO-3 were deposited *via* DCMS method in different sputtering gas ambiance. ITO-2 was obtained when the ITO-1 at 300°C was annealed at 400°C, ITO-4 was obtained when the ITO-3 at 300°C was annealed at 400°C. As seen from Figure 3, the peak intensities of ITO patterns increase with the increasing film thickness [36]. Also, this result supports the Bragg Law given by Equation 4 [31]. The more thickness of crystal ITO atoms increases, the more "n" number of ITO crystal atoms increases. This increasing n value increases the peak intensities of ITO patterns.

Figure 4 gives the crystallite structure of bilayer TiO_2 films. XRD graph in the Figure 4a gives patterns of bilayer TiO_2 films with difference thickness. The thickness of ITO layer of S3 and S4 are thicker than that of the others, so peak intensity of XRD pattern of their ITO layers at 35° value is much higher that of the others. However, peak of XRD pattern at 25° value of anatase(A)-TiO_2 crystallite structure of S1, S2 and S3 is much higher intensity than that of S3 and S4 at 25° value. TiO_2 crystallite structure of all samples is not amorphous because they were annealed at 450°C for 1 hour [37,38]. The (hkl) planes of A-TiO_2 in Figure 3 are A(101), A(004), A(200) and A(105) at 25°, 37°, 48° and 54°, respectively [39,40].

To normalise the XRD graph between 0 and 1 intensity values, intensity values in the experimental result were divided in values of normalize due to different thickness of bilayer TiO_2 films [41]. Figure 4b gives normalized XRD graphs drawn to show patterns of bilayer TiO_2 films. According to Figure 4b, while crystal structures of S1, S2 and S5 are much closer to each other, crystal structure of S3 and S4 is much closer to each other. The crystal structures of all samples are difference due to the different crystal structures of ITO layers. The crystallite sizes of anatase form of TiO_2 of S1, S2, S3, S4 and S5 are 22.40 nm, 16.43 nm, 28.98 nm, 24.63 nm and 17.14 nm , respectively. Their thicknesses given in the Table 2 decrease with decreasing crystallite size [34,35].

Each layer of S1, S2, S3, S4 and S5 has different thickness and thus the determining of their thickness is too important. For this reason, their thicknesses should be measured to observe the changes in the optical and criystallite characteristic values. Table 2 represents thicknesses of ITO and TiO_2 films coated by DCMS method. The thickness(t) and temperature(T) of DCMS-ITO and DCMS-TiO_2 films are seen in the Table 2. Thicknesses of ITO layer of S3 and S4 samples are thicker than that of S1 and S2 samples. ITO layer of S5 is commercial and its thickness is around 100 nm. The p-TiO_2 thickness of all samples could not be measured by profilometer device because of the their so rough surface and it is estimated that their thickness are around 1µm to the measured total thickness results. According to Figure 4a below, the p-TiO_2 thickness of S2 is thicker than others. The thickness of ITO layer of S5 is thinner than that of the others because it was coated by commercial device in optimum experimental laboratory conditions.

Figure 5a shows the UV-VIS absorbance spectra of bilayer TiO_2 films with difference thickness. According to Figure 5a, S3 have much more light absorption than the others because it has much thicker in comparison with the ohers. Moreover, this result verifies the Lambert-Beer Law given by Equation 2. The E_{OBG} values of S1, S2, S3, S4 and S5 determined by Equation 1 from Figure 5a are 2.90 eV, 2.92 eV, 2.79 eV, 2.88 eV and 3.25 eV, respectively. While E_{OBG} of S3 is the smallest amongst, E_{OBG} of S5 is the biggest in

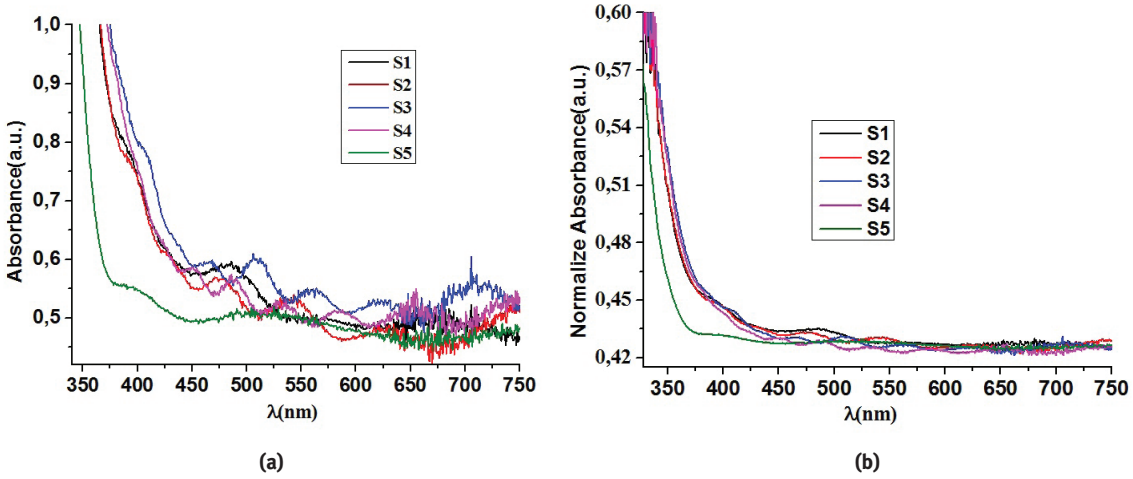

Figure 5: (a) UV-VIS **(b)** Normalized UV-VIS absorbance spectra of bilayer TiO_2 films.

Table 2: Thicknesses of both ITO and d-TiO_2 films coated by DCMS method.

Sample No	ITO coated by DCMS			d-TiO_2 coated by DCMS		
	T(°C)	t(nm)	Gas	T(°C)	t(nm)	Gas
S1	300	576	Ar+O_2	300	317	Ar
S2	400	465		400	239	
S3	300	700	Ar	300	350	Ar
S4	400	600		400	208	

their among. This difference at E_{OBG} values of bilayer TiO_2 films causes due to different E_{OBG} values of ITO layers. E_{OBG} values of S3 and S4 is smaller than that of S1, S2 and S5 because the ITO and d_TiO_2 layers of S3 and S4 are thicker than that of S1 and S2. While E_{OBG} values of all samples decrease with the increasing thickness which is due to the enlarging crystallit sizes, their light absorption increases with that [42].

Normalized UV-VIS absorbance spectra of bilayer TiO_2 films in Figure 5b was drawn due to difference thickness of each of three layer films. The E_{OBG} values of S1, S2, S3, S4 and S5 obtained from Figure 5b are 2.99 eV, 2.97 eV, 2.88 eV, 2.82 eV and 3.27 eV, respectively. After UV-VIS spectras were normalized, it was seen that E_{OBG} value of S2 was smaller than that of S1 and E_{OBG} value of S4 was smaller than that of S3, too. Spray Pyrolysis(SP) layer of S2 is thicker than that of S1 and SP layer of S4 is thicker than that of S3, too. According to Figure 5b, S2 absorbed less light when compared to S1 and S4 absorbed less light in comparison with S3, too. As a result, S2 in comparison with S1 has more light transmittance and S4 has more light transmittance than S3, too. Because p-TiO_2 as SP layers has more light transmittance than d-TiO_2 due to the Ti^{4+} ions in p-TiO_2 turning from Ti^{3+} ions in d-TiO_2 revealed with XPS [16, 20,21]. Also, S1 and S2 have much more light absorption than S3 and S4. And thus, it can be based on the Lambert-Beer Law given by Equation 2 that SP layers of S1 and S2 are thicker than that of S3 and S4. When UV-VIS values of all samples were normalized, thicknesses of ITO and d-TiO_2 layers were neglected. For this reason, the effect on light absorption of p-TiO_2 as SP layers was seen more obvious in Figure 5b. Finally, normalized absorbance of S5 and S1 is the same between 525 nm and 750 nm in the visible region because their crystal and optic properties are much close to each other. ITO structure of S2 is similar the commercial ITO structure of S5.

SEM images of top layer of S4 were given with Figure 6a, Figure 6b and Figure 6c. These images explain whether the all samples have a nanoporous (np) or non-porous (non-p) surface structure.

As seen from all images of Figure 6, bilayer TiO_2 films have not the np surface structure. Their surface structures are nonp-TiO_2 layer like dense (d) layer. The surface of samples crack due to some external factors [43] such as the temperature of hot plate in SPD mechanism when samples were deposited *via* SPD method and the solution prepared for SPD. As a result, samples have not porously structure.

4 Conclusion

Although TiO_2 films were deposited on different ITO layers in the same DCM sputtering conditions, they have different optic band gap, crystallite size and intensity of XRD patterns of A-TiO_2 due to the used ITO layers with different E_{OBG} and crystal structure properties. As a result, E_{OBG} and

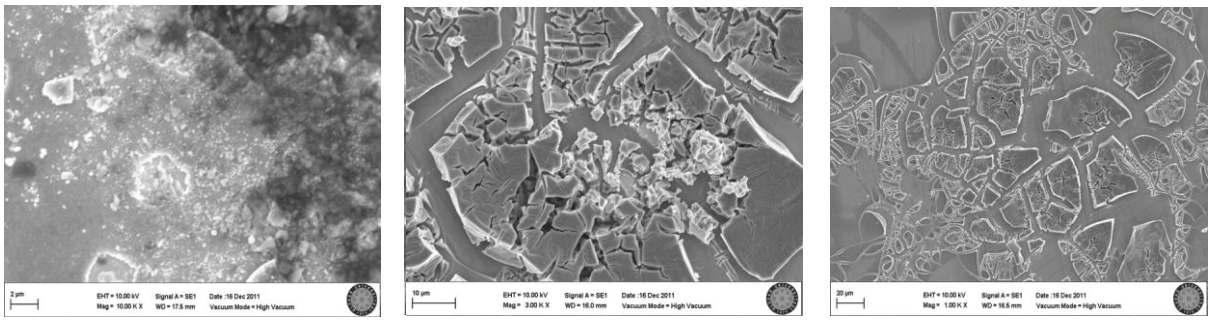

(a) (b) (c)

Figure 6: SEM images of bilayer TiO_2 films **(a)** 1000 KX **(b)** 300 KX **(c)** 100 KX.

crystal structure of TiO_2 films have changed based on that of ITO layers. The thickness, optical and crystal structure properties of ITO layers used as conductive layers are important because bilayer TiO_2 films are deposited on ITO layers. According to application field to be used TiO_2 films, ITO layers should be selected taking into consideration the optical, crystal and thickness which are important properties of application field such as E_{OBG} of TiO_2 used as media layer for transferring of electrons in the DSSCs, crystallite structure of TiO_2 used for H_2 production as photo-catalysts etc. because properties of ITO layers affect the properties of TiO_2 films.

Conflict of Interest: The authors declare that they have no conflict of interest.

References

[1] Banerjee A.N., The design, fabrication, and photocatalytic utility of nanostructured semiconductors: focus on TiO_2-based nanostructures, Nanotechnol. Sci. Appl., 2011, 4, 35-65.

[2] Aykut Y., Saquing C.D., Pourdeyhimi B., Parsons G.N., Khan S.A., Templating quantum dot to phase-transformed electrospun TiO_2 nanofibers for enhanced photo-excited electron injection, ACS Appl. Mater. Interfaces, 2012, 4, 3837-3845.

[3] Leshuk T., Linley S., Gu F., Hydrogenation processing of TiO_2 nanoparticles, Can. J. Chem. Eng., 2013, 91, 799-807.

[4] Wei A., Zuo Z., Liu J., Lin K., Zhao Y., Transport and interfacial transfer of electrons in dye-sensitized solar cells based on a TiO_2 nanoparticle/TiO_2 nanowire "double-layer" working electrode, J. Renew. Sustain. Ener., 2013, https://aip.scitation.org/doi/10.1063/1.4803525

[5] Chiarello G.L., Di Paola A., Palmisano L., Selli E., Effect of the TiO_2 Crystalline Structure on the Photocatalytic Production of Hydrogen, Photochem. Photobiol. Sci., 2011, 10, 355-360.

[6] Li R., Weng Y., Zhou X., Wang X., Mi Y., Chong R., et al., Achieving overall water splitting using titanium dioxide-based photocatalysts of different phases, Energy Environ. Sci., 2015, 8, 2377-2382.

[7] Zhang D., Jing F., Gao F., Shen L., Sun D., Zhou J., Enhanced performance of a TiO_2 ultraviolet detector modified with graphene oxide, RSC Adv., 2015, 5, 83795-83800.

[8] Hirata S., Kubota K., Jung H.H., Hirata O., Goushi K., Yahiro M., et al., Improvement of electroluminescence performance of organic light emitting diodes with a liquid emitting layer, In: Asian Conference on Organic Electronics (3-5 November 2010, Seoul, Korea) A-COE, 2010, 3-5.

[9] Al-Asbahi B.A., Jumali M.H.H., Yap C.C., Salleh M.M., Influence of TiO_2 Nanoparticles on Enhancement of Optoelectronic Properties of PFO-Based Light Emitting Diode, J. Nanomater., 2013, https://www.hindawi.com/journals/jnm/2013/561534/

[10] Aleksandrova M.P., Dobrikov G.H., Kolev G.D., Cholakova I.N., Improvement of the injection efficiency in Organic Light Emitting devices by additional spray deposited hole transporting layer, J. Sci. Eng., 2013, 1, 79-83.

[11] Radecka M., Jasiński M., Klich-Kafel J., Rekas M., Łysoń B., Czapla A., et al., TiO_2-based Nanopowders for Gas Sensor, Ceram. Mater., 2010, 62, 545-549.

[12] Anukunprasert T., Saiwan C., Traversa E., The development of gas sensor for carbon monoxide monitoring using nanostructure of Nb–TiO_2, Sci. Technol. Adv. Mater., 2005, 6, 359-363.

[13] Sivakumar A., Murugan R., Sundaresan K., Periyasamy S., UV protection and self-cleaning finish for cotton fabric using metal oxide nanoparticles, Indian J. Fibre Text. Res., 2013, 38, 285-292.

[14] Lusvardi G., Barani C., Giubertoni F., Paganelli G., Synthesis and Characterization of TiO_2 Nanoparticles for the Reduction of Water Pollutants, Materials, 2017, 10, 1-11.

[15] Haridas A.K., Gangaja B., Srikrishnarka P., Unni G.E., Nair A.S., Nair S.V., et al., , Spray pyrolysis-deposited nanoengineered TiO_2 thick films for ultra-high areal and volumetric capacity lithium ion battery applications, J. Power Sources, 2017, 345, 50-58.

[16] Xiong L-B., Li J-L., Yang B., Yu Y., Ti^{3+} in the surface of titanium dioxide: generation, properties and photocatalytic application, J. Nanomater., 2012, https://www.hindawi.com/journals/jnm/2012/831524/

[17] Berger T., Sterrer M., Diwald O., Knözinger E., Panayotov D., Thompson T.L., et al., Light-induced charge separation in anatase TiO_2 particles, J. Phys. Chem. B, 2005, 109, 6061-6068.

[18] Raman L.A., Dinanath H., Catalytic converter for ozone decomposition in aircraft cabins, J. Adv. Eng. Res., 2016, 3, 33-39.

[19] Hanaor D.A.H., Sorrell C.C., Review of the anatase to rutile phase transformation, J. Mater. Sci., 2011, 46, 855-874.
[20] Yang N., The preparation of nano composites and their applications in solar energy conversion, Springer, 2017
[21] Bugyi L., Berkó A., Óvári L., Kiss A.M., Kiss J., Enhanced dispersion and stability of gold nanoparticles on stoichiometric and reduced TiO_2(110) surface in the presence of molybdenum, Surf. Sci., 2008, 602, 1650-1658.
[22] Stamate M., Vascan I., Lazar I., Lazar G., Caraman I., Caraman M., Optical and Surface properties TiO_2 thin films deposited by dc magnetron sputtering method, J. Optoelectron. Adv. M., 2005, 7, 771-774.
[23] Singh P., Kaur D., Room temperature growth of nanocrystalline anatase TiO_2 thin films by dc magnetron sputtering, Physica B, 2010, 405, 1258-1266.
[24] Neagu R., Perednis D., Princivalle A., Djurado E., Zirconia coatings deposited by electrostatic spray deposition A chemical approach, Solid State Ion., 2006, 77, 1451-1460.
[25] Acik O.J., Junolainen A., Mikli V., Danilson M., Krunks M., Growth of ultra-thin TiO_2 films by spray pyrolysis on different substrates, Appl. Surf. Sci., 2009, 256, 1391-1394.
[26] Dhanapandian S., Arunachalam A., Manoharan C., Effect of deposition parameters on the properties of TiO_2 thin films prepared by spray pyrolysis, J. Solgel Sci. Technol., 2016, 77, 119-135.
[27] Manohari A.G., Dhanapandian S., Kumar K.S., Mahalingam T., Optimization of deposition parameters on the physical properties of TiO_2 thin films by spray pyrolysis technique, Int. J. Thin Fil. Sci. Tec., 2014, 3, 1-6.
[28] Yin X., An Q., Yu J., Guo F., Geng Y., Bian L., et al., Side-chain engineering of benzo[1,2-b:4,5b′]dithiophene core-structured small molecules for high-performance organic solar cells, Sci. Rep., 2016, 6, 1-10.
[29] Herzog B., Sengün F., Scattering Particles Increase Absorbance of Dyes – A Model Study with Relevance for Sunscreens, Photochem. Photobiol. Sci., 2013, 14, 1-25.
[30] Suryanarayana C., Norton M.G., X-Ray Diffraction A Practical Approach, Springer Sci. + Business Media, 1998
[31] Theivasanthi T., Alagar M., An Insight Analysis Nano sized powder of Jackfruit Seed, Nano Biomed. Eng., 2011, 3, 163-168.
[32] Geng S., Zhang S., Onishi H., XPS applications in thin films research, Adv. Perform. Mater., 2002, 17, 234-240.
[33] Kurdesau F., Khripunov G., da Cunha A.F., Kaelin M., Tiwari A.N., Comparative study of ITO layers deposited by DC and RF magnetron sputtering at room temperature, J. Non-Cryst. Solids, 2006, 352, 1-5.
[34] Taha H., Jiang Z.-T., Yin C.-Y., Henry D. J., Zhao X., Trotter G., et al., Novel Approach for Fabricating Transparent and Conducting SWCNTs/ITO Thin Films for Optoelectronic Applications, J. Phys. Chem. C, 2018, 122, 3014-3027.
[35] Worasukhkhung S., Pudwat S., Eiamchai P., Horprathum M., Dumrongrattana S., Aiempanakit K., Hydrophilic Property of TiO_2 Films Sputtered on Glass/ITO for Self Cleaning Glass and Heat Mirror Application, Procedia Eng., 2012, 32, 780–786.
[36] Chandrakala V., Steffy J.A.J., Bachan N., Jeyarani W.J., Tenkyong T., Shyla J.M., A Comparative Investigation of Dye-Sensitized Titanium Dioxide (TiO_2) Nanorods Grown on Indium Tin Oxide (ITO) Substrates by Direct and Seed-Mediated Hydrothermal Methods, Acta Metall. Sin., 2016, 29, 457-463.
[37] Rozenberga-Voska L., Grabis J., Synthesis and Photocatalytic Activity of Modified TiO_2 Thin Films Prepared by Spray Pyrolysis, Solid State Phenom., 2017, 267, 3-6.
[38] Ohtani B., Ogawa Y., Nishimoto S., Photocatalytic Activity of Amorphous–Anatase Mixture of Titanium(IV) Oxide Particles Suspended in Aqueous Solutions, J. Phys. Chem. B, 1997, 101, 3746-3752.
[39] Ma Y.-J., Lu F., Xiang B.-X., Zhao J.-L., Ruani S., Fabrication of TiO_2 thin films with both anatase and rutile structures together using the ion-implantation method, Opt. Mater. Express, 2018, 8, 532-540.
[40] Collazzo G.C., Jahn S.L., Carreño N.L.V., Foletto E.L., Temperature and Reaction Time Effects on the Structural Properties of Titanium Dioxide Nanopowders Obtained via The Hydrothermal Method, Braz. J. Chem. Eng., 2011, 28, 265-272.
[41] Aji B.B., Shih S.J., Pradita T., Controlled crystal phase of TiO_2 by spray pyrolysis method, J. Phys. Conf. Ser., 2017, 817, 1-6.
[42] Yılmaz M., Eker Y.R., Synthesis of Graphene via Chemical Vapour Deposition on Substrates with Different Thicknesses, Anadolu Univ. J. Sci. Technol., 2017, 18, 289-300.
[43] Ennaceri H., Boujnah M., Taleb A., Khaldoun A., Sáez-Araoz R, Ennaoui A., et al., Thickness effect on the optical properties of TiO_2 anatase thin films prepared by ultrasonic spray pyrolysis: Experimental and ab initio study, Int. J. Hydrogen Energ., 2017, 42, 19467-19480.
[44] Perednis D., Gauckler L.J., Thin Film Deposition Using Spray Pyrolysis, J. Electroceramics, 2004, 14, 103-111.